JOURNAL OF THERMOPHYSICS AND HEAT TRANSFER
Vol. 14, No. 1, January–March 2000

Experimental Investigation of Surface Reactions in Carbon Monoxide and Oxygen Mixtures

Steven Sepka,* Yih-Kanq Chen,† and Jochen Marschall‡
NASA Ames Research Center, Moffett Field, California 94035-1000
and
Richard A. Copeland§
SRI International, Menlo Park, California 94025-3493

During hypersonic entry into the CO_2 atmosphere of Mars, competing exothermic chemical reactions may occur on a spacecraft heatshield surface. Two possible surface reactions are $O + O \rightarrow O_2$ and $CO + O \rightarrow CO_2$. The relative importance of these reactions on quartz is investigated using a diffusion tube side-arm reactor together with two-photon laser-induced fluorescence for both O and CO species detection. The experiments show 1) that the presence of CO in the gas phase does not significantly affect the oxygen recombination reaction on quartz and 2) that the gas-phase CO concentration is not significantly altered by the presence of atomic oxygen. These results indicate that for our experimental conditions the dominant surface reaction on quartz in oxygen-carbon monoxide mixtures is $O + O \rightarrow O_2$. Current heating computations for Martian entries assume CO oxidation to be fully catalytic. The resulting entry heating values are significantly higher than those computed using the assumption of fully catalytic oxygen recombination. The data presented here indicate that the assumption of fully catalytic CO oxidation may be overly conservative for heatshield sizing purposes.

Nomenclature

C = species concentration, m^{-3}
D = diffusion coefficient, m^2-s^{-1}
J = mass flux, kg-m^{-2}-s^{-1}
K = surface reaction rate coefficient, m-s^{-1}
M = molar mass, kg-mol^{-1}
P = pressure, Pa
R = side-arm radius, m
T = temperature, K
$\bar{v}$ = average thermal speed, m-s^{-1}
x = side-arm axial coordinate, m
Z = collision partner
γ = recombination coefficient
ρ = density, kg-m^{-3}
σ = standard deviation
χ = mole fraction

Subscripts

CO = carbon monoxide
CO_2 = carbon dioxide
i = reaction index
m = mean
O = atomic oxygen
O_2 = molecular oxygen
$[s]$ = surface site

Received 6 May 1999; presented as Paper 99-3629 at the AIAA 33rd Thermophysics Conference, 28 June–1 July 1999, Norfolk, VA; revision received 9 August 1999; accepted for publication 19 August 1999.

*NRC Fellow, Thermal Protection Materials and Systems Branch; ssepka@mail.arc.nasa.gov. Member AIAA.
†Aerospace Engineer, Thermal Protection Materials and Systems Branch; ykchen@mail.arc.nasa.gov.
‡Senior Research Scientist, Thermosciences Institute, Eloret Corporation; jmarschall@mail.arc.nasa.gov. Senior Member AIAA.
§Senior Chemical Physicist, Molecular Physics Laboratory; rich@mplvax.sri.com.

Introduction

DURING hypersonic planetary entry a high-temperature shock wave that forms along the vehicle forebody can dissociate molecular species present in the atmosphere. Exothermic surface recombination reactions involving these dissociated species can contribute significantly to the aeroconvective heating of the vehicle. During Earth entry, the dominant atmospheric species to dissociate are molecular oxygen and nitrogen. The importance of surface catalyzed reactions to Earth reentry heating was shown in a series of flight experiments on the Space Shuttle. Adjacent tiles in the heatshield attained significantly different surface temperatures depending on the catalycity of their surface coating.[1–3]

Many experimental investigations of the surface recombination rates of oxygen and nitrogen atoms on representative thermal protection system (TPS) materials have been made over the last several decades, both in the laboratory and in large-scale arc jet facilities (e.g., see Refs. 1–6 and citations therein). As a result, some experimentally based estimates of O + O and N + N recombination on different materials are available in the literature. These estimates can be incorporated in computer codes designed to calculate Earth entry heating.

For Mars or Venus entries, the computation of realistic catalytic heating contributions is more problematic. Both atmospheres are predominately carbon dioxide. Carbon dioxide can dissociate into CO, O, and C, in proportions depending on the energy dissipated during the entry. The dissociation of CO into O and C requires about twice as much energy as the dissociation of CO_2 into CO and O. For a typical Mars entry, the dissociation of CO is small, and the concentration of C near the heat shield surface is calculated to be negligible.[7] Surface reactions that can contribute to heating are those involving CO and O. Two competitive reactions are possible, $CO + O \rightarrow CO_2$ and $O + O \rightarrow O_2$. Presently there is very little experimental information available to assess the relative importance of each reaction for TPS materials. Mars entry heating computations that include catalytic effects usually assume fully catalytic CO oxidation; this assumption gives the maximum possible heating contribution.[7–10]

We report the results of several experiments on surface catalytic effects in carbon monoxide–oxygen mixtures. The purpose of these experiments is twofold: first, to develop a sound experimental approach to study surface catalytic effects on TPS materials in carbon

monoxide–oxygen mixtures and, second, to investigate the relative importance of the two competitive surface reactions $CO + O \rightarrow CO_2$ and $O + O \rightarrow O_2$.

Experiment

A schematic diagram of the experimental apparatus is given in Fig. 1. The experiments were conducted in a dead-end, diffusion tube side-arm reactor. This type of reactor was first introduced by Smith[11] for the study of low-catalycity materials and has been used extensively over the years (see Refs. 5 and 6 and citations therein). The steady-state gas-phase concentrations of reactant species vary as a function of axial location down the side-arm tube due to losses by surface reactions on the tube walls. The catalycity of the wall surface can be determined by matching solutions of the appropriate species diffusion equation(s) to experimentally measured species gradients. For the simplest case of one specie recombining via a single first-order surface reaction, a one-dimensional species diffusion analysis (assuming negligible end effects) leads to the familiar one-dimensional exponential decay[11]

$$C(x) = C_0 \exp\left[-\sqrt{\bar{\nu} R\gamma / 2D}(x/R)\right] \tag{1}$$

Here C_0 is the specie concentration at $x = 0$ and the recombination coefficient γ is defined as the fraction of reactant specie that strikes the wall and disappears from the gas phase. For multiple reacting species and multiple competing surface reactions, the diffusion analysis is more complicated, and the definitions of recombination coefficients change; a detailed description of a particular reactor model for the carbon monoxide–oxygen system is given in a later section.

The approach taken in this study was to look for changes induced in the concentration of one of the species by the addition of the other into the reactor. Two complementary experiments were conducted. First, the decay of the O-atom concentration down the length of side arm was measured with and without the presence of CO in the reactor, and second, the concentration of CO in the side arm was measured with and without the presence of atomic oxygen. In the former experiments, a change in the O-atom decay down the side arm with the addition of CO would indicate that CO surface reactions are taking place. A decrease in the O-atom loss rate would suggest that CO molecules are tying up surface recombination sites, whereas an increase in the O-atom loss rate would suggest that O-atoms are being removed by the CO oxidation reaction. In experiments of the second type, a change from a uniform CO concentration to a decay down the side arm when O-atoms are introduced would indicate that the $CO + O \rightarrow CO_2$ surface reaction is consuming CO molecules.

Previous laboratory studies worked with dissociated CO_2 flows.[12,13] However, the composition of such flows is uncertain. In the present work, atomic oxygen was generated by flowing O_2 through a microwave discharge, and CO was introduced downstream. The amounts of CO and O_2 entering the reactor were measured using calibrated flow meters, and the amount of atomic oxygen created in the discharge was estimated from steady-state pressure measurements with the discharge on and off. Experiments confirmed that there was negligible dissociation of any CO that back-diffused into the discharge. No O atoms could be detected when CO was introduced downstream of a helium discharge.

Two-photon laser-induced fluorescence (LIF) was used for both atomic oxygen[14,15] and carbon monoxide[16,17] species detection. In this technique, a ground state oxygen atom or carbon monoxide molecule is excited to an upper state by absorption of two UV photons. The excited atom or molecule subsequently decays radiatively via photon emission from the upper state to an intermediate lower energy state. The strength of this fluorescence is directly proportional to the ground state number density in the gas volume illuminated by the laser, provided that ionization, amplified spontaneous emission, and collisional losses from the upper state are minimized. Two-photon LIF enables spatially resolved species selective measurements with minimal intrusion. These characteristics are significant advantages over traditional measurement techniques employed in surface recombination studies, such as calorimeters or thermocouples that respond to net heating effects and cannot be used to detect separate reaction paths.

Details of the species detection schemes, the reactor, the optical layout, and the experimental procedures are given in the subsections that follow.

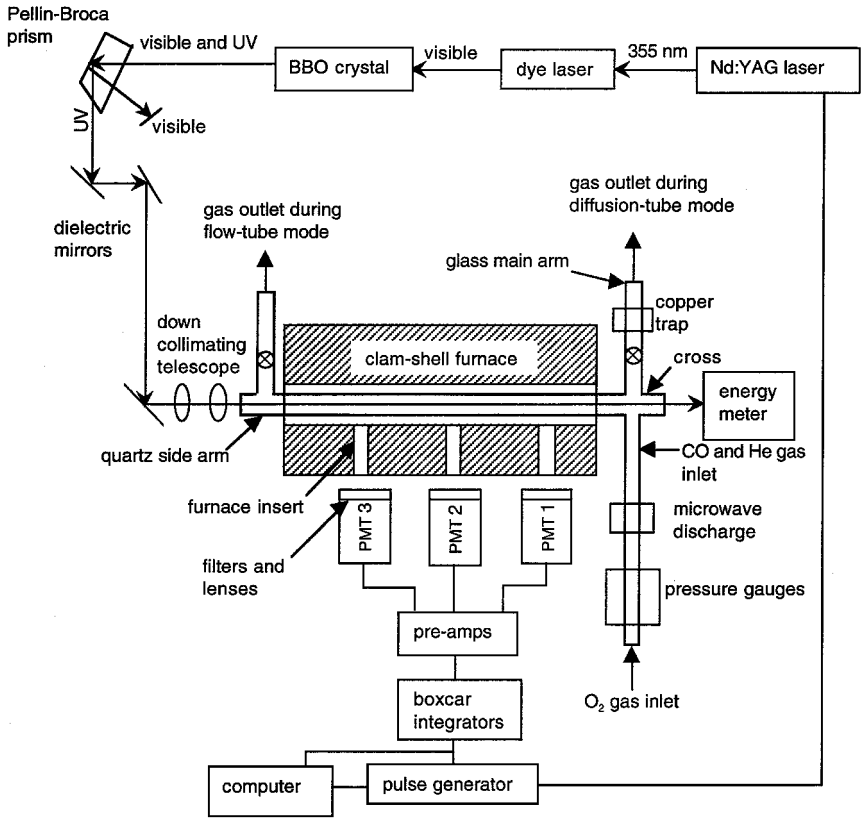

Fig. 1 Schematic diagram of the experimental apparatus.

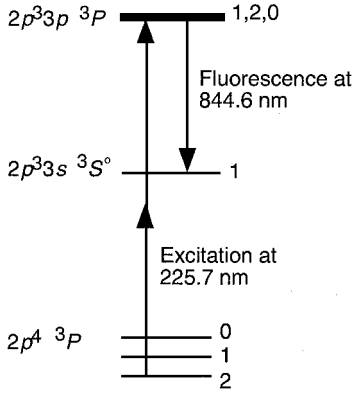

Fig. 2 Energy level diagram of atomic oxygen illustrating the states and transitions relevant for two-photon LIF.

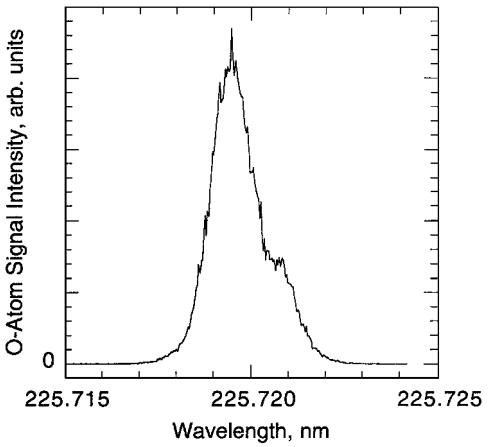

Fig. 3 Excitation scan of atomic oxygen originating from the ground, $J=2$ state. Shoulder appearing at ~225.721 nm is due to the fine-structure levels of the excited state.

Atomic Oxygen Detection

The relevant energy level diagram for oxygen atom detection is shown in Fig. 2. The oxygen atom ground state has three fine-structure components with differing angular momentum, $J=2$, 1, or 0, that are populated at thermal equilibrium according to the Boltzmann distribution. The $J=2$ component has the highest relative population over the temperature range of the experiment, ranging from 74% at 300 K to 64% at 700 K. UV radiation near 225.7 nm was used to excite the ground state oxygen via the $3p\,^3P_{1,2,0} \leftarrow 2p\,^3P_2$ two-photon transition.[14,15] The excited atoms fluoresce in the infrared at 844.6 nm via the $3p\,^3P_{1,2,0} \rightarrow 3s\,^3S^0_1$ transition. Because the three fine-structure components of the $3p\,^3P$ state are all within 1 cm^{-1} of each other, only a single heavy solid line is shown in Fig. 2 for this state.

Figure 3 shows an excitation scan through the resonance associated with the $3p\,^3P_{1,2,0} \leftarrow 2p\,^3P_2$ transition of atomic oxygen. During experiments in which the O-atom concentration was monitored, the excitation wavelength was tuned to maximize the fluorescence signal.

Carbon Monoxide Detection

Ground state carbon monoxide molecules were excited using UV light near 230 nm via the $B\,^1\Sigma^+ \leftarrow X\,^1\Sigma^+(0,0)$ two-photon transition.[16,17] This excitation wavelength corresponds to a transition from the lowest lying ($v''=0$) vibrational level of the $X\,^1\Sigma^+$ ground state to the lowest lying ($v'=0$) vibrational level of the $B\,^1\Sigma^+$ excited state. Some of the CO molecules in the $B\,^1\Sigma^+$ state fluoresce in the visible and near-infrared region via the $B\,^1\Sigma^+ \rightarrow A\,^1\Pi$ transition, as shown in Fig. 4. Multiple fluorescence wavelengths arise because CO in the $B\,^1\Sigma^+(v'=0)$ state can fluoresce to several different vibrational levels of the $A^1\Pi$ state (primarily the $v''=0$–6 levels).

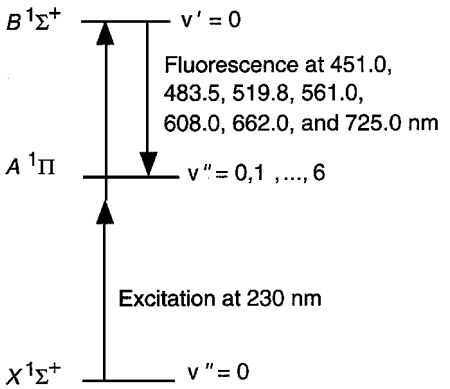

Fig. 4 Energy level diagram of carbon monoxide illustrating the states and transitions relevant for two-photon LIF.

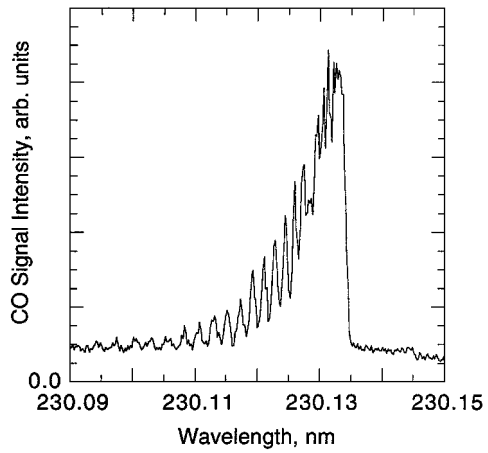

Fig. 5 Two-photon LIF signal from carbon monoxide as a function of laser wavelength at a temperature of 295 K and a pressure of 61 Pa; features are due to the Q-branch of the B-X(0, 0) transition.

Figure 5 shows the Q-branch ($\Delta J=0$) excitation spectrum of CO, as the UV wavelength was scanned over the $B\,^1\Sigma^+ \leftarrow X\,^1\Sigma^+(0,0)$ transition. Transitions from different thermally populated rotational levels of ground state CO give rise to the observed structure in the two-photon LIF spectrum. For CO detection, the excitation wavelength was tuned near 230.13 nm to maximize the fluorescence.

Reactor

The reactor consisted of a glass main arm and a quartz side arm joined by a quartz cross. Approximately 18 in. (0.47 m) of the side-arm tube were enclosed in a Lindberg electric clam-shell furnace. Gases were introduced into the main arm upstream of the cross. By a simple adjustment of valves (see Fig. 1) the side arm could be turned into either a dead-end diffusion tube or a flow tube. In the diffusion tube mode, gases were pulled through the main arm by a Varian V-90 turbomolecular pump backed with a mechanical pump. In the flow tube mode, gases were pulled through the side arm by a high-capacity mechanical pump. A fluorinated pump oil (Fomblin) was used in both mechanical pumps to avoid explosion hazards.

A microwave discharge was positioned on the main arm upstream of the cross. Molecular oxygen was introduced into the reactor upstream of the discharge while gases such as helium and carbon monoxide were introduced between the cross and the discharge. The power delivered to the microwave discharge was typically 40 W. From pressure measurements made with the discharge on and off, the O_2 dissociation fraction at this power level was estimated to be in the range of 1–3%. Because the discharge received a constant power input and was operated under steady-state temperature and

gas flow conditions, the O_2 dissociation (as monitored by LIF) was essentially constant during any given experimental run.

Gas Handling

Gas flow was measured using calibrated Tylan mass flow meters, and gas pressure was measured using a Baratron capacitance manometer gauge. The gases used in these experiments were oxygen (99.998%), helium (99.999%), and a mixture of 2.0% carbon monoxide in helium.

The $O + O_2 + Z \rightarrow O_3 + Z$ gas-phase three-body reaction becomes significant at pressures above ~65 Pa (~0.5 torr) (Ref. 18). To eliminate the influence of this gas-phase reaction on species concentration profiles, the total reactor pressure was always kept below 53 Pa (0.4 torr). The $O + O + Z \rightarrow O_2 + Z$ reaction, although approximately five times faster than the ozone producing reaction at room temperature,[19] is less important because of the low O-atom concentrations present in the system. The reaction $CO + O + Z \rightarrow CO_2 + Z$ is much slower than the $O + O_2 + Z \rightarrow O_3 + Z$ reaction[20] and is insignificant in the pressure range of our experiments.

Because only 1–3% of the molecular oxygen flow was dissociated, the partial pressure of atomic oxygen was quite small. The experiments were designed to add CO to the reactor in comparable concentrations to the O atoms. Because of the low partial pressures of atomic oxygen, it was necessary to buffer the CO in He to obtain a bulk flow rate sufficiently large for accurate measurement. During the experiments the oxygen flow rate was fixed, and either pure He or the 2.0% CO in He mixture was added to raise the reactor pressure to a particular value.

The existence of iron carbonyl impurities in bottled CO is well known.[17,20] When using CO, the gas was first heated to a temperature above 200 C to decompose any iron carbonyl impurities acquired from the walls of the gas cylinder and then cooled back to room temperature prior to entering the main arm.

Optical Layout

A frequency tripled Continuum NY81 Nd:YAG laser was used to pump a Continuum ND60 dye laser to provide tunable blue radiation near 452 nm for oxygen atom detection and near 460 nm for carbon monoxide detection. Both wavelengths were produced using Coumarin 460 laser dye. The blue light was frequency doubled by passing it through a beta-barium borate crystal. Residual blue light in the beam was separated from the desired UV radiation using a Pellin–Broca prism. Several dichroic mirrors and a down-collimating Galilean telescope were used to direct the beam through a quartz window oriented at Brewster's angle and down the centerline of the side arm. The laser pulse energy was monitored with a Molectron J3-09 pyroelectric energy meter that intercepted the beam as it exited the reactor through a similar Brewster's angle window located on the cross.

Fluorescence was detected at normal incidence to the side-arm tube by three photomultiplier tubes (PMTs) spaced 8.9 cm apart. The PMTs are labeled PMT1, PMT2, and PMT3 in Fig.1; PMT1 is the nearest PMT to the cross. A wedge-shaped refractory insert was constructed to allow optical access while the furnace was closed and operating. This refractory insert had 1-cm-diam optical ports lined with quartz tubes to view the centerline of the side-arm tube along its axis. The light emerging from the ports was collected using gated, red-sensitive, photomultiplier tubes (Hamamatsu R636 tubes with a C1392 sockets).

For O-atom fluorescence detection, the PMTs were fitted with narrowband interference filters centered at 845 nm with a full width at half maximum (FWHM) bandpass of ~3 nm. For CO fluorescence detection, initial measurements were made using a 400-nm long-pass and 500-nm short-pass filter combination on PMT1, a bandpass filter centered at 483 with a FWHM of 10 nm on PMT2, and a 450-nm long-pass and 550-nm short-pass filter combination on PMT3. During the course of the experiments, 450-nm long-pass and 550-nm short-pass filter combinations were also obtained for PMT1 and PMT2.

Because of variations in PMT response, filter transmission characteristics, and optical alignment, the fluorescence detection sensitivities at the three locations along the side arm differed. The relative fluorescence detection sensitivities at the three locations were determined by collecting fluorescence from a uniformly distributed specie. For CO detection, this could be achieved trivially by filling the reactor with a CO–He mixture. For O-atom detection, the side arm was converted to flow tube mode so that axial O-atom concentration gradients could be minimized. With a sufficiently high pumping speed, axial O-atom concentration gradients produced by surface reactions were largely overcome by convection (flow). The relative detection sensitivities were used to correct measured signals obtained in the diffusion tube experiments. These calibrations were made frequently throughout the experiments because the relative detection sensitivities were strong functions of the laser beam alignment through the side arm.

Care was taken to record background baselines for each test and subtract them from the data. For O-atom detection, background signals were relatively small and arose predominantly from scattered laser light and electronic noise found in the data acquisition instruments. For CO detection, the dominant background signal contribution was from fluorescence of the quartz windows on the side arm. This background fluorescence was large and could not be filtered out because the spectral ranges of the quartz and the CO fluorescence overlap. During experiments employing CO detection, measurements were also made without CO in the reactor to obtain accurate background fluorescence signals for later subtraction from the data.

Data Acquisition

A Stanford Research Systems data acquisition system was used along with a personal computer to collect, process, and store output signals from the energy meter and the PMTs. The data acquisition system consisted of an SR240 preamplifier, several SR250 gated integrators, and an SR 245 computer interface, all housed in an SR280 mainframe. The Nd:YAG laser, the gated PMT, and the data acquisition system were triggered at 10 Hz and timed with respect to one another using a Stanford Research System DG535 digital delay and pulse generator.

The data collection for a typical test consisted of acquiring approximately 250 bins of data on four channels, that is, the energy meter and three PMTs, with each bin containing the mean signal from 10 laser shots. The appropriate baseline offset was subtracted from each bin, and the average signal and associated standard deviation were calculated for each channel. The average PMT signals and the standard deviations were then corrected for the relative detection sensitivities at the different locations. The final corrected PMT signals were directly proportional to the species concentration at each detection location.

Experimental Results

Experimental results are presented in Figs. 6–8. Figures 6–8 show relative species concentrations as a function of distance along the side arm. Species concentrations are normalized to one at the first measurement location, which is also taken as the zero of the dimensionless axial coordinate x/R. The error bars in Figs. 6–8 are the standard deviations σ (calculated as described earlier) and represent the scatter in the data collected during a single run. The standard deviations of the means σ_m are about a factor of 15 smaller, where $\sigma_m \equiv \sigma/\sqrt{\text{number of data points}}$. Variations in averaged concentration measurements obtained during sequential test runs (under identical reactor conditions) were consistent with σ_m values. The data points in Figs. 6–8 are slightly offset to separate individual error bars.

The experimental conditions corresponding to Figs. 6–8 are listed in Table 1. The mixture compositions at the entrance to the side arm were calculated from measured gas flows and an O_2 dissociation fraction of 1.5%. The effective multispecies diffusion coefficients of O and CO were estimated from Wilke's approximation[21] using the binary diffusion coefficients given by Marrero and Mason[22] and the calculated mole fractions given in Table 1. The uncertainty in the

Table 1 Experimental conditions at the entrance to the diffusion side arm

	Figure 6				Figure 7		Figure 8			
Parameter	With CO	Without CO	With CO	Without CO	With O	Without O	With CO	Without CO	With O	Without O
T, K	295	295	623	623	292	292	295	295	298	298
P, Pa	41.5	41.5	41.6	41.6	49.9	50.7	49.6	50.5	49.6	49.2
χ_{He}	0.902	0.922	0.902	0.923	0.326	0.337	0.315	0.341	0.318	0.316
χ_{O_2}	0.077	0.075	0.077	0.075	0.648	0.656	0.658	0.633	0.656	0.678
χ_O	0.0023	0.0023	0.0024	0.0023	0.020	——	0.020	0.019	0.020	——
χ_{CO}	0.019	——	0.019	——	0.0067	0.0069	0.0065	——	0.0066	0.0065
$D_{O\text{-}M}$, $cm^2\text{-}s^{-1}$	1990	2070	7370	7640	805	——	825	838	846	——
$D_{CO\text{-}M}$, $cm^2\text{-}s^{-1}$	1440	——	5160	——	529	530	542	——	556	554

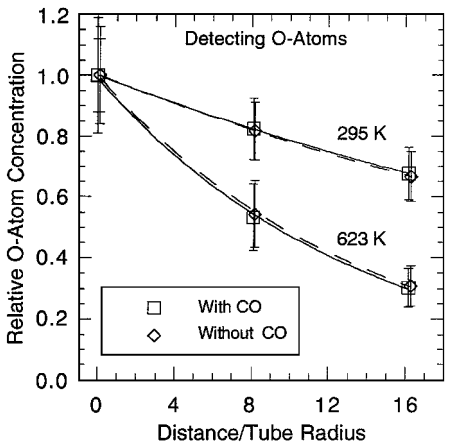

Fig. 6 Relative O-atom concentration vs location along the diffusion tube side arm; solid and dashed lines are exponential fits to the data obtained with CO and without CO, respectively.

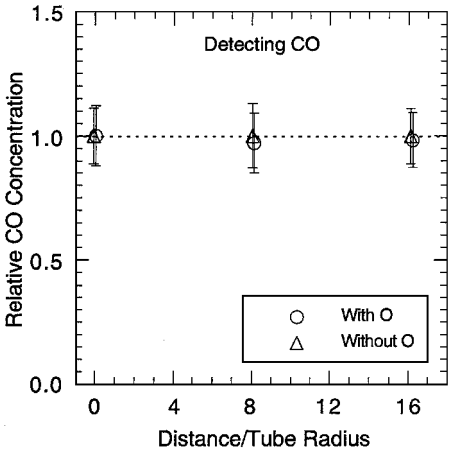

Fig. 7 Relative CO concentration vs location along the diffusion tube side arm at 295 K. (Dotted horizontal line at 1 is given as an aid to the eye.)

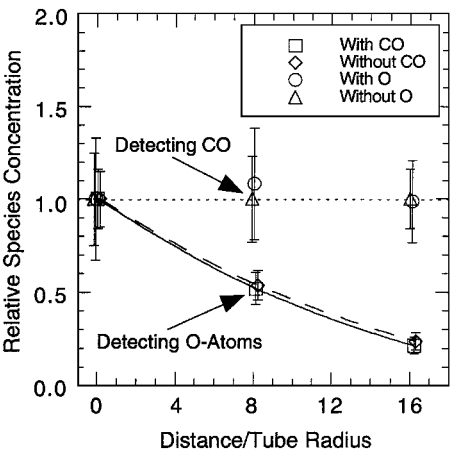

Fig. 8 Relative species concentration vs location along the diffusion tube side arm at 295 K; 1.27-cm-wide Inconel 617 strip positioned between PMT2 and PMT3: solid and dashed curves are fits to the data obtained with CO and without CO, respectively. (These curves and the dotted horizontal line at 1 are given as aids to the eye.)

temperature and pressure measurements is less than 5%. The largest experimental uncertainty is associated with the O_2 dissociation fraction. Estimates of O_2 dissociation based on pressure measurements are most likely low and could be off by a factor of 2 or more. Thus, whereas the O_2, He, and CO mole fractions have uncertainties on the order of 5–10%, the O mole fraction could be uncertain by factors of 2 or more. The absolute value of an individual diffusion coefficient is accurate to about ±20%; the ratio of diffusion coefficients for two similar mixtures is much more accurate.

The first set of experiments was to determine whether the addition of CO to the reactor would enhance or diminish the removal of O atoms from the gas phase. To this end, it was desired to keep the O-atom diffusion coefficient in the gas mixture approximately constant while adding CO in excess over O to drive CO surface reactions if they were significant.

Experiments were conducted in two gas mixtures, the first mixture containing only helium and oxygen and the second mixture containing, in addition, carbon monoxide. Both mixtures were at a total pressure of ~41 Pa (~0.31 torr). The gas-flow rates, in standard cubic centimeters per minute, were 1.79 for O_2 and 21.5 for He in the first mixture and 1.79 for O_2, 20.5 for He, and 0.42 for CO in the second mixture. The calculated mole fractions of O atoms and CO molecules in the second mixture, at the entrance to the side arm, were ~0.0023 and 0.019, respectively. Even with the large uncertainty in the O-atom mole fraction, the CO molecules were clearly in excess relative to the O atoms during this experiment. The O-atom diffusion coefficients in the two mixtures are calculated to differ by less than 5%.

Figure 6 shows the decay of the O-atom concentration down the side arm, for measurements made with each gas mixture at two different temperatures. The O-atom concentration profile along the side arm was consistent with an exponential decay. The catalycity of quartz increases with temperature, resulting in the greater rate of O-atom loss at 623 K as compared to 295 K. Figure 6 clearly shows that there were no significant differences in O-atom decay in the two different mixtures at either 295 or 623 K, even though CO was in excess over O by a factor of ~8 in the second mixture. Although relative O-atom concentrations are plotted in Fig. 6, note that the absolute magnitude of the O-atom LIF signal was similar in both mixtures, indicating no significant changes in the absolute O-atom concentrations. Similar measurements, made at intermediate temperatures and on different days, consistently found that the addition of CO to the reactor had no effect on O-atom losses from the gas phase.

The results of this first set of experiments can be interpreted in two ways: Either 1) CO surface reactions were insignificant and

the observed O-atom decay was caused solely by oxygen atom recombination in both mixtures, or 2) the CO and oxygen surface reactions, along with the relative surface coverage of O atoms and CO molecules, can combine to give the same net O-atom removal down the side arm. Clearly the first interpretation is more reasonable than the second because the second requires a fortuitous combination of reaction kinetics. If the latter interpretation were correct, the gas-phase CO concentration should also decay down the side arm (when the CO- and O-atom concentrations are similar.)

A second set of experiments was conducted to look for such a CO decay. In these experiments, the CO concentration was monitored while the microwave discharge was turned on and off to control the presence of atomic oxygen in the reactor. The flow rates of O_2 and the He–2.0%CO mixture were set so that the concentration of atomic oxygen when the discharge was turned on was in excess over CO. The removal of CO from the gas phase via the CO + O→ CO_2 surface reaction, thus, would not be limited by the availability of atomic oxygen in the mixture.

Typical results are shown in Fig. 7. The reactor pressure was ~50 Pa (~0.38 torr). The gas-flow rates into the reactor were 14.0, 6.71, and 0.14 standard cm^3/min for O_2, He, and CO, respectively. The mole fractions of atomic oxygen and CO when the discharge was on were calculated to be ~0.020 and 0.0067, respectively. Thus, the O-atom concentration at the entrance to the side arm was clearly in excess over the CO concentration. The difference in the effective multispecies diffusion coefficient of CO with or without the presence of atomic oxygen in the mixture was calculated as less than 1%.

Figure 7 compares the uniform CO concentration obtained with the discharge off to the CO concentrations measured when the discharge was on. The measured concentration profiles were practically identical. The CO concentration clearly did not decay down the side arm when atomic oxygen was introduced. The absolute magnitude of the CO LIF signal was similar with the discharge on or off indicating no CO consumption by O atoms. This measurement was repeated several times on different days. Because of signal-to-noise limitations, some scatter of relative concentrations about unity was observed. Nevertheless, all experiments of this type provided complementary evidence that, for our experimental conditions, oxygen removal from the gas phase via the CO oxidation reaction was not competitive with the oxygen recombination reaction.

The catalycity of quartz for oxygen recombination is relatively low. To check if a more catalytic surface for oxygen recombination would alter the results, several experiments were conducted with a 1.27-cm-wide Inconel 617 strip lining the inside of the diffusion side arm between PMT2 and PMT3. Both O and CO were detected in separate experiments of the type described earlier. Representative results are presented in Fig. 8. The total pressure and the composition of the gas mixtures were kept very similar to those for Fig. 7. Once more the introduction of CO caused no significant changes in the O-atom decay curve, nor did the presence of atomic oxygen alter the uniform concentration of CO down the side arm.

Finally, because we detected no changes in the gas-phase CO concentration in our experiments, the question of CO detection sensitivity may be raised. In particular, the $B\,^1\Sigma^+ \leftarrow X\,^1\Sigma^+(0, 0)$ transition is allowed by both single-photon and two-photon selection rules. The radiative deexcitation of the excited CO molecule directly to its ground state with the emission of a ~113-nm UV photon can lead to radiation trapping. Radiation trapping increases the apparent lifetime of the excited state and may degrade the resolution of any CO concentration gradients. When detecting CO in our experiments, the partial pressure of CO was about 0.33 Pa (~2.5 mtorr). Some radiation trapping was certainly present at this CO pressure[23]; however, the effect of radiation trapping upon CO concentration measurements was not significant. A linear relationship between signal strength and CO concentration was experimentally confirmed over the CO partial pressure range of our measurements. Additionally, to confirm our ability to detect gas-phase CO changes due to surface reactions, several experiments were conducted at ~200 C with a platinum foil between PMT2 and PMT3. The surface reaction of O_2 and CO on platinum to form CO_2 at this temperature is well known.[24] In these experiments, the CO concentration was monitored as O_2 was introduced into the reactor, and the loss of CO from the gas phase was easily detected.

Reactor Model

A numerical model was constructed to simulate multispecies diffusion and surface reaction phenomena in the diffusion tube side arm. This model was consistent with the general approach employed for past Martian entry heating computations that included CO and O surface catalysis.[7,9,10,25] Surface reactions are presumed to follow first-order kinetics and to be irreversible. Reaction products leave the surface instantaneously and only (potentially) reacting species may attach to the surface. Five possible surface reactions are included in the model:

$$\mathrm{O} + [s] \rightarrow \mathrm{O}_{[s]}, \qquad i = 1 \tag{2a}$$

$$\mathrm{CO} + \mathrm{O}_{[s]} \rightarrow \mathrm{CO}_2 + [s], \qquad i = 2 \tag{2b}$$

$$\mathrm{O} + \mathrm{O}_{[s]} \rightarrow \mathrm{O}_2 + [s], \qquad i = 3 \tag{2c}$$

$$\mathrm{CO} + [s] \rightarrow \mathrm{CO}_{[s]}, \qquad i = 4 \tag{2d}$$

$$\mathrm{O} + \mathrm{CO}_{[s]} \rightarrow \mathrm{CO}_2 + [s], \qquad i = 5 \tag{2e}$$

The rate coefficient for the ith reaction is given by

$$K_i = \gamma_i(\bar{v}_i/4) \tag{3}$$

where γ_i is defined as the fraction of gaseous specie striking the wall that undergoes the ith reaction. The sum of all γ_i for a particular specie cannot exceed one, leading to the restrictions

$$\gamma_1 + \gamma_3 + \gamma_5 \leq 1 \tag{4}$$

$$\gamma_2 + \gamma_4 \leq 1 \tag{5}$$

The mass fluxes due to surface reactions are balanced by diffusion. A body-fitted co-ordinate system is used:

$$J_\mathrm{O} = -\rho D_\mathrm{O} \nabla \chi_\mathrm{O} = -(K_1 + K_3 + K_5)\rho_\mathrm{O} \tag{6}$$

$$J_\mathrm{CO} = -\rho D_\mathrm{CO} \nabla \chi_\mathrm{CO} = -(K_2 + K_4)\rho_\mathrm{CO} \tag{7}$$

$$J_{\mathrm{O}_2} = -\rho D_{\mathrm{O}_2} \nabla \chi_{\mathrm{O}_2} = \left[K_3(M_{\mathrm{O}_2}/M_\mathrm{O})\right]\rho_\mathrm{O} \tag{8}$$

$$J_{\mathrm{CO}_2} = -\rho D_{\mathrm{CO}_2} \nabla \chi_{\mathrm{CO}_2} \tag{9}$$

$$= \left[K_2(M_{\mathrm{CO}_2}/M_\mathrm{CO})\right]\rho_\mathrm{CO} + \left[K_5(M_{\mathrm{CO}_2}/M_\mathrm{O})\right]\rho_\mathrm{O} \tag{10}$$

For steady-state conditions, the fraction of the surface covered by each reactant must remain constant. This leads to further restrictions on γ_i:

$$\gamma_1 = \gamma_2(\rho_\mathrm{CO}/\rho_\mathrm{O})(M_\mathrm{O}/M_\mathrm{CO})^{\frac{3}{2}} + \gamma_3 \tag{11}$$

$$\gamma_4 = \gamma_5(\rho_\mathrm{O}/\rho_\mathrm{CO})(M_\mathrm{CO}/M_\mathrm{O})^{\frac{3}{2}} \tag{12}$$

Note that, if the multispecies formulation is reduced to a binary mixture, for example, O and O_2, the restrictions of Eqs. (4) and (10) lead to $\gamma_1 = \gamma_3 \leq \frac{1}{2}$. Thus, the single recombination coefficient γ used in the simple exponential decay of Eq. (1) is equivalent to the sum of $\gamma_1 + \gamma_3$ in the present model formulation.

Gas-phase reactions were negligible under the conditions of the side-arm experiment and were omitted from the model. In addition to the species involved in the surface reactions of Eqs. (2), the gas-phase diffusion model also includes helium. Whereas helium does not participate in any reactions, its presence does modify species diffusion rates significantly. The multispecies diffusion equations were solved using the bifurcation diffusion approximation[26] and a finite volume differencing scheme analogous to that used in the GIANTS code.[25]

The reactor model was used to calculate room temperature O and CO concentration profiles along the side arm for the gas-phase mixtures of Figs. 6 and 7. To compute concentration profiles, three of the five γ_i must be specified. The remaining two γ_i are then determined by Eqs. (10) and (11). It is plausible that the quartz surface was predominantly covered by O atoms not CO molecules. If CO molecules were covering significant fractions of the surface, a decrease in O-atom loss down the side arm would be expected with the addition of CO to the reactor, and no such decrease was observed in the experiments. Thus, we take $\gamma_4 = 0$, and $\gamma_5 = 0$ follows from Eq. (11). (Similar assumptions about surface coverage were made in Ref. 13.) The room temperature recombination coefficient of O on quartz in a binary O–O_2 mixture[5] is on the order of 1×10^{-4}. We, therefore, set γ_3 to 5×10^{-5}, so that in the absence of CO, $\gamma_1 + \gamma_3 = 1 \times 10^{-4}$.

O and CO concentration profiles computed as a function of γ_2/γ_3 are shown in Figs. 9 and 10, respectively. For each value of γ_2/γ_3, coefficient γ_1 was determined by Eq. (10). A comparison of the experimental (Fig. 6) and computed (Fig. 9) O-atom decay curves indicates that γ_2 must be more than one order of magnitude smaller than γ_3 for reasonable agreement. Moreover, the model results for both O and CO concentration profiles are in good agreement with the experimental results in the limit of $\gamma_2/\gamma_3 = 0$. Note that a fully catalytic CO oxidation condition ($\gamma_2 = 1$ and $\gamma_2/\gamma_3 = 20{,}000$) would lead to concentration profiles completely incompatible with our measurements.

Whereas the particular set of γ_i fixed in these simulations was not unique, substitution of other reasonable values does not alter the general conclusions. In all cases, the model simulations support the basic result of our experiments: oxygen recombination dominates over CO oxidation.

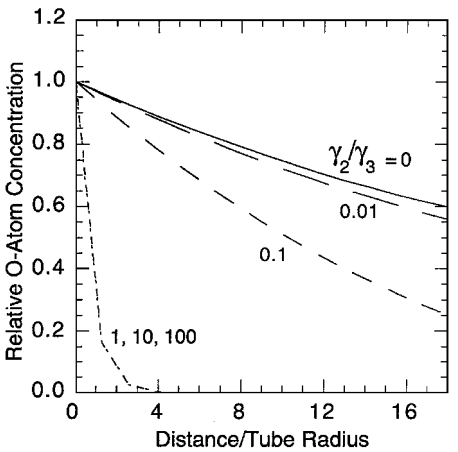

Fig. 9 Model computations of O-atom decay profiles as a function of γ_2/γ_3 for the experimental conditions of Fig. 6 at 295 K.

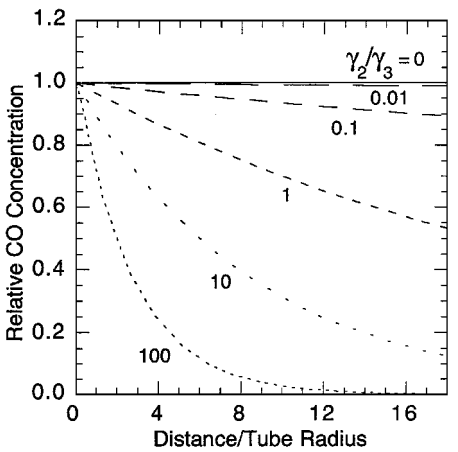

Fig. 10 Model computations of CO decay profiles as a function of γ_2/γ_3 for the experimental conditions of Fig. 7 at 295 K.

Discussion

A recent Russian study[13] examined the catalycity of quartz surfaces in subsonic flows of dissociated carbon dioxide. Stagnation point heat transfer measurements were made, and these were compared with numerical simulations of the flow and the probe thermal response to extract a net effective recombination coefficient for all surface reactions. Because heat flux measurements are not species selective, the relative importance of various possible surface reactions, such as O + O → O_2, CO + O → CO_2, and C + O → CO, could not be assessed. However, the general finding of the study was that catalytic heating contributions in dissociated carbon dioxide and dissociated oxygen were similar. This result is consistent with our finding that O-atom recombination is the dominant surface reaction on quartz in mixtures of O and CO.

Note that the rate constant of the gas-phase three-body reaction CO + O + Z → CO_2 + Z is two to three orders of magnitude slower than that of O + O + Z → O_2 + Z (Refs. 19 and 20). To the extent that a low-catalycity surface is similar to an inert reaction partner, the gas-phase reaction data also suggest that oxygen recombination would dominate over carbon monoxide oxidation. The slow reaction rate of CO with O in the gas phase is attributed to the spin mismatch between the triplet ^3P ground state of atomic oxygen and the singlet $X\,^1\Sigma^+$ ground state of CO. Reactions involving excited states of O or CO may be substantially quicker; however, they do not play an important role in our experiments. The lowest lying triplet state of CO ($a\,^3\Pi$) is about 6 eV above the ground state[27] and cannot be thermally populated. The lowest lying singlet state of atomic oxygen (^1D) is about 2 eV above the ground state, and thermal population of this state in our experiments was also negligible. It is possible that a small number of ^1D O-atoms were created in the discharge; however, these excited atoms are rapidly quenched by oxygen molecules[18] and would not persist in the gas phase long enough to interact with the CO molecules injected downstream of the discharge.

The results of the present work suggest that Mars entry heating computations based on fully catalytic CO + O → CO_2 recombination may be overly conservative. Figure 11 shows the effect of different surface catalysis assumptions on heating predictions computed for the maximum stagnation point heating time of the Mars Pathfinder entry (66 s). Computations were made using the programs and methodology outlined in Ref. 25, with the inclusion of the O + O → O_2 surface reaction. The predicted heating differences between surfaces modeled as fully catalytic for CO_2 production or fully catalytic for O_2 production are significant. Any initial TPS sizing based on entry heating calculations assuming fully catalytic CO oxidation rather than fully catalytic oxygen recombination will necessarily lead to increased vehicle weight. Initial TPS sizing using

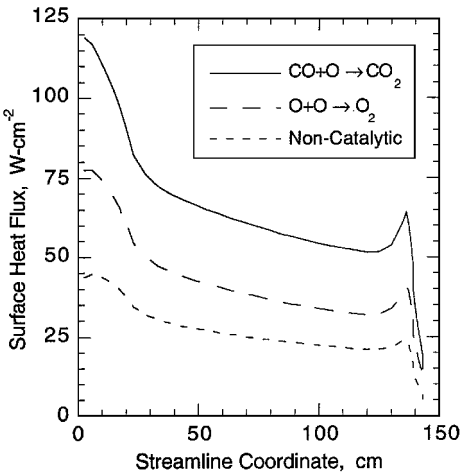

Fig. 11 Surface heat flux calculations for the peak stagnation point heating time (66 s) during the Mars Pathfinder entry, assuming fully catalytic CO_2 production, fully catalytic O_2 production, or a noncatalytic surface.

fully catalytic oxygen recombination heating estimates should still be conservative. No real surface is fully catalytic. Furthermore, in actual application, surface heating is also reduced by any ablation or pyrolysis that may occur.

Conclusion

Experimental results indicate that oxygen recombination is much more important than carbon monoxide oxidation on quartz surfaces (at least over the pressure and temperature range so far explored). The recombination rate of oxygen atoms was essentially unaffected by the presence of carbon monoxide in the gas phase. Likewise, the presence of oxygen atoms in the gas phase did not significantly change observed carbon monoxide concentrations. Room-temperature experiments on Inconel 617—a material known to be more catalytic for oxygen recombination than quartz—showed similar results. A numerical model was constructed to simulate multispecies diffusion and surface reaction in the reactor. The model formulation and numerical solution were consistent with the methodology of past Mars entry catalytic heating computations. Representative computations confirm that the experimentally observed O and CO concentration profiles were inconsistent with significant surface catalyzed CO oxidation. The results of the present work suggest that Mars entry heating computations based on fully catalytic $CO + O \rightarrow CO_2$ recombination may be overly conservative. Clearly, further work must be done to extend the temperature and pressure ranges of these experiments and to extract numerical values of γ for actual TPS materials of interest.

Acknowledgments

We thank David Stewart for motivating this research and Joan Pallix, Frank Milos, and Stephen Walch for helpful discussions. The contributions of J. Marschall and R. Copeland were supported by NASA Contract NAS2-14031 to Eloret Corporation. S. Sepka acknowledges the support of the National Research Council through their fellowship program.

References

[1]Stewart, D. A., Rakich, J. V., and Lanfranco, M. J., "Results of a Flight Experiment on the Catalytic Efficiency of the Space Shuttle Heat Shield," AIAA Paper 82-0944, June 1982.

[2]Stewart, D. A., Rakich, J. V., and Lanfranco, M. J., "Catalytic Surface Effects on Space Shuttle Thermal Protection System During Earth Entry Flights STS-2 Through STS-5," *Shuttle Performance: Lessons Learned*, NASA CP-2283, Pt. 2, Oct. 1983, pp. 827–846.

[3]Stewart, D. A., Rakich, J. V., and Chen, Y.-K., "Flight Experiment Demonstrating the Effect of Surface Catalysis on the Heating Distribution Over the Space Shuttle Heat Shield," *Orbiter Experiments (OEX) Aerothermodynamics Symposium*, CP-3248, NASA, Pt. 2, 1995, pp. 677–701.

[4]Stewart, D. A., "Surface Catalytic Efficiency of Advanced Carbon Carbon Candidate Thermal Protection Materials for SSTP Vehicles," NASA TM-110383, Feb. 1996.

[5]Pallix, J. B., and Copeland, R. A., "Measurement of Catalytic Recombination Coefficients on Quartz Using Laser-Induced Fluorescence," *Journal of Thermophysics and Heat Transfer*, Vol. 10, No. 2, 1996, pp. 224–233.

[6]Marschall, J., "Experimental Determination of Oxygen and Nitrogen Recombination Coefficients at Elevated Temperature Using Laser-Induced Fluorescence," AIAA Paper 97-3879, Aug. 1997.

[7]Chen, Y.-K., Henline, W. D., Stewart, D. A., and Candler, G. V., "Navier–Stokes Solutions with Surface Catalysis for Martian Atmospheric Entry," *Journal of Spacecraft and Rockets*, Vol. 30, No. 1, 1993, pp. 32–42.

[8]Rochelle, W. C., Kirk, B. S., and Starbranch, E. S., "Aeroheating Analysis for Mars TransHab Vehicles, Volume I—Methodology and Results," Lockheed Martin Space Mission Systems and Services, LMSMSS-32724, Houston, TX, Feb. 1998.

[9]Micheltree, R. A., and Gnoffo, P. A., "Wake Flow About a MESUR Mars Entry Vehicle," AIAA Paper 94-1958, June 1994.

[10]Gupta, R. N., Lee, K. P., and Scott, C. D., "Aerothermal Study of Mars Pathfinder Aeroshell," *Journal of Spacecraft and Rockets*, Vol. 33, No. 1, 1996, pp. 61–69.

[11]Smith, W. V., "The Surface Recombination of H Atoms and OH Radicals," *Journal of Chemical Physics*, Vol. 11, No. 3, 1943, pp. 110–125.

[12]Xu, J., "Kinetic Study of Surface Recombination of CO Molecules and O Atoms," *The Recombination of O-O, N-N, and CO-O Species by Oxygen Atoms on Surfaces of Materials Used in Space Vehicles*, prepared by Y.-C. Kim, Dept. of Chemical Engineering, Stanford Univ., Final Rept. NCA2-504, Stanford, CA, 1991.

[13]Kolesnikov, A. F., Pershin, I. S., Vasil'evskii, S. A., and Yakushin, M. I., "Study of Quartz Surface Catalycity in Dissociated Carbon Dioxide Subsonic Flows," AIAA Paper 98-2847, June 1998.

[14]Bischel, W. K., Perry, B. E., and Crosley, D. R., "Detection of Fluorescence from O and N Atoms Induced by Two-Photon Absorption," *Applied Optics*, Vol. 21, No. 8, 1982, pp. 1419–1429.

[15]Bamford, D. J., Jusinski, L. E., and Bischel, W. K., "Absolute Two-Photon Absorption and Three-Photon Ionization Cross Sections for Atomic Oxygen," *Physical Review A: General Physics*, Vol. 34, No. 1, 1986, pp. 185–198.

[16]Aldén, M., Wallin, S., and Wendt, W., "Applications of Two-Photon Absorption for Detection of CO in Combustion Gases," *Applied Physics B*, Vol. 33, 1984, pp. 205–208.

[17]Tjossem, P. J. H., and Smyth, K. C., "Multiphoton Excitation Spectroscopy of the $B\ ^1\Sigma^+$ and $C\ ^1\Sigma^+$ Rydberg States of CO," *Journal of Chemical Physics*, Vol. 91, No. 4, 1989, pp. 2041–2048.

[18]DeMore, W. B., Sander, S. P., Golden, D. M., Hampson, R. F., Kurylo, M. J., Howard, C. J., Ravishankara, A. R., Kolb, C. E., and Molina, M. J., "Chemical Kinetics and Photochemical Data for Use in Stratospheric Modeling, Evaluation Number 12," Jet Propulsion Lab., Publication 97-4, California Inst. of Technology, Pasadena, CA, Jan. 1997, p. 93.

[19]Baulich, D. L., Drysdale, D. D., Duxbury, J., and Grant, S. J., *Evaluated Kinetic Data for High Temperature Reactions*, Vol. 3, Butterworth, Boston, 1976, p. 33.

[20]Slanger, T. G., Wood, B. J., and Black, G., "Kinetics of $O(^3P) + CO + M$ Recombination," *Journal of Chemical Physics*, Vol. 57, No. 1, 1972, pp. 233–238.

[21]Wilke, C. R., "Diffusional Properties of Multicomponent Gases," *Chemical Engineering Progress*, Vol. 46, No. 2, 1950, pp. 95–104.

[22]Marrero, T. R., and Mason, E. A., "Gaseous Diffusion Coefficients," *Journal of Physical and Chemical Reference Data*, Vol. 1, No. 1, 1972, pp. 3–118.

[23]Dotchin, L. W., Chupp, E. L., and Pegg, D. J., "Radiative Lifetimes and Pressure Dependence of the Relaxation Rates of Some Vibronic Levels in N_2^+, N_2, CO^+, and CO," *Journal of Chemical Physics*, Vol. 59, No. 8, 1973, pp. 3960–3967.

[24]Bonzel, H. P., and Ku, R., "Carbon Monoxide Oxidation on a Pt(110) Single Crystal Surface," *Journal of Vacuum Science and Technology*, Vol. 9, No. 2, 1972, pp. 663–667.

[25]Milos, F. S., Chen, Y.-K., Congdon, W. M., and Thornton, J. M., "Mars Pathfinder Entry Temperature Data, Aerothermal Heating, and Heatshield Material Response," AIAA Paper 98-2681, June 1998.

[26]Bartlett, E. P., Kendall, R. M., and Rindal, R. A., "An Analysis of the Coupled Chemically Reacting Boundary Layer and Charring Ablator. Part IV: A Unified Approximation for Mixture Transport Properties for Multicomponent Boundary-Layer Applications," NASA CR-1063, June 1968.

[27]Krupenie, P. H., *The Band Spectrum of Carbon Monoxide, National Standard Reference Data Series*, Vol. 5, National Bureau of Standards, 1966.